



Detection of Delaminations in Concrete Plates Using a Laser Ablation Impact Echo Technique

Johannes F. Scherr¹ · Jochen Kollofrath¹ · John S. Popovics³ · Benjamin Bühling² · Christian U. Grosse¹

Received: 16 December 2021 / Accepted: 23 December 2022 / Published online: 5 January 2023
© The Author(s) 2023

Abstract

This study investigates the non-destructive detection of delaminations in concrete plates using non-contact laser ablation, instead of the conventional hammer excitation, as part of the impact echo method. We performed tests on five concrete specimens of different sizes, two of which contained artificial delaminations. A range of steel ball hammers was used as reference impulse sources, the responses of which were compared with wave excitation generated by a 7 ns pulsed 1064 nm Nd:YAG laser with 150 mJ pulse energy. Signals were recorded by surface-mounted accelerometers and two contactless methods: microphones and a laser Doppler vibrometer. The laser generates frequencies across a broad range of frequencies (0 to 150 kHz) but with much less energy than the hammers' narrower frequency spectra; the laser pulse energy transferred into the specimen is 0.07 mJ, corresponding to about 0.5 % of the impulse source energy. Because of this, the thick intact plates' characteristic thickness stretch resonance frequency can be reliably detected by the hammer excitations but not when using laser excitation. However, the laser can excite low-frequency flexural vibration modes over a shallow delamination at 3 cm depth. The low-frequency flexural vibration results are verified by numerical natural frequency analysis.

Keywords Concrete testing · Defect detection · Lamb waves · Impact echo · Non-destructive testing · Vibration

1 Background Information

Impact echo (IE) is a well-established non-destructive testing method for delamination detection and thickness measurement of concrete structures, especially where access is only available from one side [1]. In many applications, manual application of the mechanical impact event required in IE suffices because the area that needs to be tested is sufficiently small, and inspection time is not a critical factor. In applications such as concrete pavements and concrete bridge decks, however, manual testing is not feasible. In most cases, the area is vast, and testing time must be kept as short as possible because road closures must be minimized. Several IE testing

devices have been developed over recent years and successfully applied in small and large surveys [2–4]. Common to all these devices is that they rely on a mechanical impact event, limiting the testing speed and preventing them from being used in running traffic. To overcome the problem of limited maximum speed because of the need for mechanical impact events, we investigated a laser impulse source as a fast and contactless alternative. In general, pulsed lasers can achieve high excitation repetition rates to the MegaHertz range from a single pulse. The nanosecond laser pulse duration can, in theory, excite frequencies up to several MegaHertz, values generally used for ultrasonic testing of metal elements but which thus far have not been used in impact echo testing of thick concrete plates [5]. The advantages of contactless application, high repetition rates, and broad frequency content are offset by the disadvantage of expected lower energy content for each pulse provided by the laser source. We compared steel ball hammers and laser excitation on five test specimens to determine if and how laser ablation can be used for impact echo testing in concrete. The objective of the current study is to apply the research on contactless acoustics in cementitious materials from previous studies to the non-destructive testing method impact echo. Such studies, for instance, have

✉ Johannes F. Scherr
j.scherr@tum.de

¹ Chair of Non-Destructive Testing, Technical University of Munich, Franz-Langinger-Straße 10, 81241 Munich, Germany

² Bundesanstalt für Materialforschung und -Prüfung (BAM), Unter den Eichen 87, 12205 Berlin, Germany

³ Department of Civil and Environmental Engineering, University of Illinois at Urbana-Champaign, 205 N. Mathews Ave., Urbana, IL 61801, USA

investigated the attenuation and scattering of laser-generated ultrasound in concrete [6, 7]. Mori et al. [8] in 2002 studied contactless defect detection in concrete using shock waves generated by a shock tube and showed that they could detect shallow defects. Studies from Dai et al. [9, 10] investigated an electric spark in combination with a parabolic reflector to focus the pressure wave onto the surface, excite the thickness resonance frequency and gain the resonance frequency in a fully contactless way. A review of current contactless NDT methods is given in Kaczmarek et al. [11] from 2016, describing the benefits and challenges of non-contact sensing with a focus on ultrasonic transducers. The work reported here explores in detail the practical application of laser-based impact echo for defect detection in concrete in terms of frequency content and energy input of the excitations.

1.1 Impact Echo

The impact echo testing method was developed in the 1980s by the National Institute of Standards and Technology and Cornell University as a non-destructive testing technique for plate-like concrete structures, such as bridge decks [1]. The standard impact echo testing method uses a mechanical impact, usually from a hammer, to excite elastic waves that set up vibrations. The first symmetric lamb mode (S1-ZGV), also called the thickness stretch resonance frequency, is excited in an intact plate, with the vibration motion having an out-of-plane displacement that is, therefore, easily measured on the surface. The thickness stretch resonance frequency can be well approximated if the plate thickness and P-wave velocity of the concrete are known. Over a delaminated area, i.e., an area in which a horizontal crack divides an intact plate into two, low-frequency flexural vibration modes may be excited in addition to the thickness resonance frequency. The time domain signals are measured and transformed into the frequency domain. Detailed theory can be found in [12]. Oh & Popovics [13, 14] found that the flexural vibration frequency for significant near-surface delaminations (greater than 160 mm × 160 mm) falls below 6 kHz in most cases. In contrast, the thickness stretch resonance frequency does not usually fall below 6 kHz because the plate thickness, for example, of a bridge deck, usually is in the range of (20 to 30) cm. In most cases, it is thus sufficient to look at the low-frequency responses to identify delamination defects, but deep-lying delaminations could be missed in cases involving thick bridge decks. In our experiments, the excited signals are recorded with surface-mounted accelerometers and in a non-contact manner using microphones and a laser Doppler vibrometer (LDV). To compare the excitation of the hammer and laser, we need to compare the energy transfer into the specimen and the frequencies excited in the specimen. Suppose we assume the hammer represents the free fall of an object. In that case, the energy

transfer can be simplified as the potential energy of the hammer assuming a perfectly elastic collision where all of the hammer's kinetic energy is transferred into the specimen without internal losses: $E_{pot} = m \times g \times \Delta h$, where m is the mass of the hammer, g is the acceleration due to gravity, and Δh is the height difference between the height from which the object was dropped and the height to which it rebounded. This approximation was also described by Sansalone in 1997 [15]. Based on the thickness of the concrete plate to be tested, steel ball hammers with a tip diameter of (5 to 20) mm are commonly used in IE testing. When dropped from a height of 50 cm, energy in the range of (1 to 40) mJ is converted and transferred into the specimen. The frequencies created in the specimen are almost exclusively related to the diameter of the steel tip and range up to 50 kHz [16]. A large-diameter steel tip will have a longer contact time (t_c) with the surface, and the generated elastic waves will have a high energy broad pulse with a narrow frequency band. By comparison, a small diameter steel tip will excite a wide frequency band with a narrow pulse and lower energy. Best practice examples show that frequencies up to $f_{max} = 1.25/t_c$ can be used [17].

1.2 Laser-Generated Elastic Waves

There are three known ways in which laser impulses are used to generate elastic waves in solids. The first is laser ablation, where a small part of the surface is ablated, i.e., blasted off due to thermal stresses created by the laser light. The detailed photophysical and photochemical mechanisms of ablation are not described here, but the interested reader is referred to Bäuerle and von Allmen [18, 19]. The second is the thermoacoustic effect, in which a sub-volume of a sample is rapidly heated up by laser irradiation resulting in thermal expansion and, consequently, a generation of elastic waves in the specimen [20, 21]. The third is the photoacoustic effect, in which the interaction of photons with the specimen surface generates elastic waves [22]. The highest energy transfer into the specimen is achieved using ablation because of the recoil effect from the ablated material. The laser used in this experiment is a 1064 nm Nd:YAG laser, generally used for laser cleaning applications, with a nominal pulse energy of 300 mJ and a pulse duration of 7 ns. The minimum energy needed to achieve an ablation is called the *ablation threshold* and depends on the laser wavelength, pulse duration, and material properties [23, 24]. Highly absorbent materials such as metals require lower energy input to achieve ablation, while more transparent materials such as glass and ceramics require higher energy input. During ablation, the material typically undergoes a phase change, depending on the laser and material parameters, from the solid phase to a melt or directly to a gas and plasma phase [23]. The recoil created by the ablation injects energy into the specimen. However, we cannot use the same assumption for mechanical hammer impacts,

namely that the potential pulse energy (E_{pot}) is fully converted into elastic wave energy. One reason is that the 7 ns laser pulse duration does not result in a 7 ns long energy input into the material. Wilsch [25] showed with Laser Induced Breakdown Spectroscopy (LIBS) experiments that a plasma could exist for 100 ms after the start of interaction with the laser. The contact time is therefore not equal to the pulse duration, but rather is longer. Mikami et al. [26] also found that the theoretically expected excited high frequencies generated by laser ablation cannot be measured in a concrete plate. Furthermore, when the surface is impinged by laser irradiation, the electrons of the substrate material (concrete) absorb the energy and ionize the atoms, leading to the formation of a plasma. This plasma shields the substrate from the further incoming laser light and thereby reduces the received energy [18].

2 Materials and Methods

Laser and hammer excitation are compared with respect to their ability to detect delaminations and excited frequencies as well as energy transferred into the specimen. If not stated otherwise in the following, the recorded analog signals were digitized using a TiePie Handyscope HS4, sampling at a rate of 500 kHz for a period of 40 ms, and stored on a hard drive.

2.1 Sensors and Sources

The setup for laser IE testing has a mirror arm for positioning. A 200 mm focusing lens aligns the laser beam perpendicular to the concrete surface. We measured a pulse energy of 150 mJ at the aperture with an optical power meter, suggesting that half of the energy is lost in the mirror arm. Five different sensors were used in the study at varying specimens. In the surface setup, with the excitation generated on the surface of the specimens using the 5 mm, 8 mm, and 10 mm steel ball hammers as well as the laser source, signals were recorded with the PCB 325C33 accelerometer, PCB 352M66 accelerometer, Polytec laser Doppler vibrometer (LDV) (OFV-5000 Vibrometer with OFV-505 sensor head), PCB 378B02 condenser microphone at 3 cm separation from the point of excitation. In the backside setup, where the excitation is generated on the surface of the 15 cm cube specimen using 5 mm, 8 mm, and 10 mm steel balls as well as the laser source, signals are recorded on the backside using the PCB 352C33 accelerometer and LDV. However, it was impossible to measure any signal from the laser-excited waves using the LDV on the backside of the specimen, so those data are not reported. At the steel-reinforced slab, we used the Olsen CTG-2 concrete thickness gauge for impact echo testing. A description of the sensors used in the experiments is listed in Table 1.

2.2 Test Execution

The recorded time signals were transformed in the frequency domain and integrated with respect to frequency. We relate the integrated area, i.e., the area under the curve up to 250 kHz, to the potential energy to find a value for the energy transferred from the laser to the specimen. As we use different mechanical impact sources, hammers, and steel balls, we only work with the steel ball impact energy because this can be precisely calculated. To quantify the laser energy transferred into the specimen, we make use of the calculated kinetic energy of the hammer and compare the signals from hammer impact and laser ablation.

For the surface test configuration, we measure the signals on the intact plate surface next to the excitation with a surface-mounted accelerometer, a microphone, and the LDV. For the backside test configuration, we measure the signals on the backside of a 15 cm concrete cube, where the signals are generated by dropping steel balls on the opposing surface of the cube. The rebound height of the steel balls was video recorded in slow-motion, and its values were subtracted from the drop height with an estimated read-off error of ± 2 cm. The concrete cube was alternatively used because we could not measure on the backside of the intact plate as the plate was lying on the ground. Signals are transformed into the frequency domain and then integrated with respect to frequency using the trapezoidal integration sub-routine in MATLAB. The integrated values from the hammers can then be related to the previously calculated kinetic impulse energy of the hammers. The integrated values of frequency spectra generated by the laser are then used to determine the relative laser energy. We can expect the surface waves to have higher amplitude and frequency content than the body waves that travel through 15 cm of concrete until they reach the backside sensors. This is due to damping, scattering, and geometrical spreading of the body waves in the specimen. Frequency contents are estimated from the frequency spectra. The two setups on the surface and the backside allow us to compare frequency and energy content nearby the excitation point and at a 15 cm distance. The expected thickness resonance frequencies for the concrete specimens were calculated using the free software Dispersion Calculator (DC) [27]. To excite the thickness resonance frequency of the specific specimen, frequencies that match resonance frequency are required with high energy content. For the delaminated plate, intact plate, and cube specimen, which were all made from the same concrete batch, the Poisson's ratio was 0.2, Young's modulus 42 GPa, density 2400 kg / m³, and P-wave velocity 4400 m / s.

The 3 cm deep delamination in the delaminated plate vibrates in the frequency range of (1 to 5) kHz. A numerical vibration analysis was run to compare experimental results with simulated vibrations. The eigenfrequencies for

Table 1 List of sources, sensors, and samples with dimensions and expected thickness stretch resonance frequency

Sources	Sensors	Samples	Dimensions ($l \times w \times h$) (cm)	Resonance frequency (Hz)
Laser, Steel ball hammers (5, 8, 10) mm	PCB 352C33 (Acc), PCB 378B02 (Mic), LDV	Intact plate	100 × 100 × 15	14 400
		Delaminated plate	100 × 100 × 15	N/A
		Delamination	40 × 40 × 3	70 000
Laser, Olson CTG-2 gauge	PCB 352C33 (Acc), PCB 378B02 (Mic), LDV	Steel-reinforced Slab	120 × 120 × 20	10 500
Laser, Steel ball hammers (5, 8, 10) mm	PCB 352C33 (Acc), PCB 352M66 (Acc), PCB 378B02 (Mic), LDV	Step wedge 1	40 × 40 × 8	26 600
		Step wedge 2	40 × 40 × 12	17 760
		Step wedge 3	40 × 40 × 16	13 320
Laser, Steel balls (5, 8, 10) mm	PCB 352C33 (Acc), LDV	Cube	15 × 15 × 15	13 700*

*Denotes an eigenfrequency of the cube specimen

the delaminated plate part 40 cm × 40 cm × 3 cm with constrained (fixed) sides were numerically simulated in COMSOL Multiphysics®. No excitation is given as input; only the undamped free oscillation of the plate based on the material properties is simulated. The predefined mesh-setting *Extra fine* with a maximum element size of 1.4 cm consisting of 27 744 tetrahedral elements. A finer mesh was tested but only increased computing time and did not change the results. Computing time for the first six natural frequencies was 20 s on a workstation.

2.3 Samples

Overall, five specimens are used for testing in this study with different purposes. The intact and delaminated concrete plates were used to investigate the detection capability of a shallow delamination at 3 cm depth. We measured the thickness resonance frequency at the intact plate and compared the results to the delaminated plate. The step wedge specimen was tested to see if the laser can excite thickness resonance vibrations in the single steps of varying thickness. The steel-reinforced slab specimen served the purpose of a deep-lying delamination and an empty tendon duct and was a fair comparison to the shallow delamination of the delaminated specimen. The cube specimen was used for energy and frequency comparison of hammer and laser. A description of each specimen and, if available, its resonance frequency is listed in Table 1

The intact concrete plate specimen has dimensions (1 × 1 × 0.15) m. A drawing of the plate and the measurement profile is given in Fig. 1 (left). The plate was struck along the y-axis in a common offset configuration with 10 cm source and receiver spacing, meaning that the source and receiver are moved together 10 cm after each measurement.

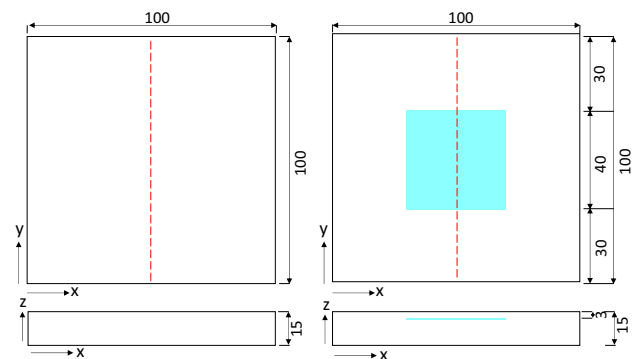


Fig. 1 Drawing of the intact plate (left) and delaminated plate (right). Artificial 3 mm thick Styrofoam delamination located at a 3 cm depth, indicated in turquoise. Red dashed lines denote the 2-D profile line. Dimensions in cm

The delaminated concrete plate specimen is of the same size as the intact plate but contains a (40 × 40 × 3) mm Styrofoam plate at 3 cm depth. This is the standard design of an artificial delamination as similar setups are chosen in Zhu & Popovics and Oh et al. [13, 28]. The acoustic impedance contrast of styrofoam and concrete $r \approx -1$ and thus comparable to the impedance contrast of concrete and air. Therefore, we consider the plate a valid model of a delamination caused by a horizontal air-filled crack. Laser and hammer excitation was deployed along a profile across the plate center [Fig. 1 (right)]. A photo showing the testing setup using the laser along with the PCB 352C33 accelerometer and PCB 378B02 microphone is displayed in Fig. 2.

The steel-reinforced slab specimen is a concrete plate with dimensions (1.20 × 1.20 × 0.20) m and contains several artificial features. It incorporates a Styrofoam plate at 15 cm depth, an empty metal tendon duct, and two steel bar reinforcement mats (see Fig. 3). The same specimen is used

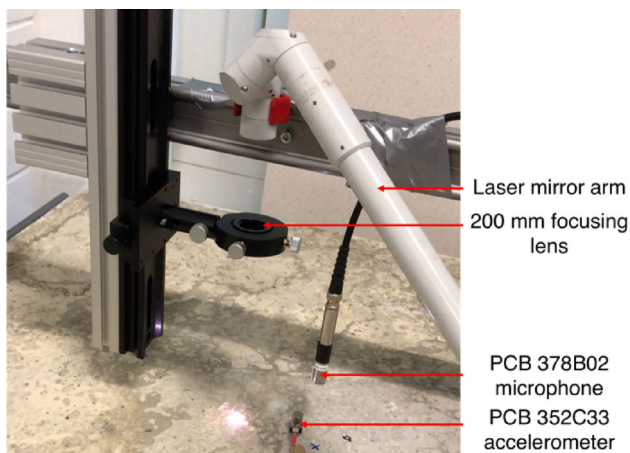


Fig. 2 Soliton LT-300 laser used for IE testing. The laser mirror arm positions the laser beam through a focusing lens on the concrete surface. PCB 352C33 accelerometer and PCB 378B02 microphone are used to record signals on the surface and in the air, respectively. The bright spot on the surface is the ablation that is visible to the human eye

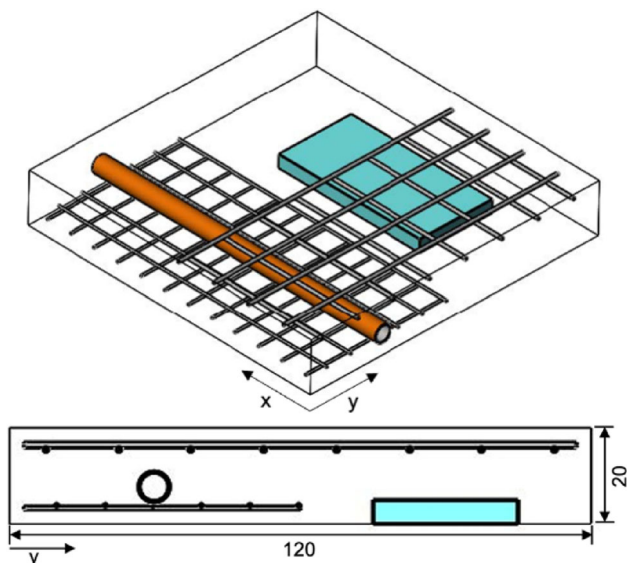


Fig. 3 Steel-reinforced slab specimen with built-in features. 5 cm thick Styrofoam delamination at 15 cm depth indicated in turquoise. Empty metal tendon duct indicated in orange. Upper and lower reinforcement layers partially cover the tube and delamination. Dimensions are shown in cm

by Niederleithinger et al. [29] for muon tomography imaging of its interior, whose paper also includes photos of the specimen. The calculated thickness resonance frequency is approximately 10.5 kHz. The data reported here for this sample were collected by Aßman and Bühling [30] using the Olson CTG-2 system with a 5 cm testing grid spacing. Signals were recorded for 8 ms with a sampling rate of 1 MHz.

The step wedge specimen is a 2 m long and 40 cm wide concrete wedge with five steps of varying thickness. The first step is 8 cm high, and the step height increases in 4 cm

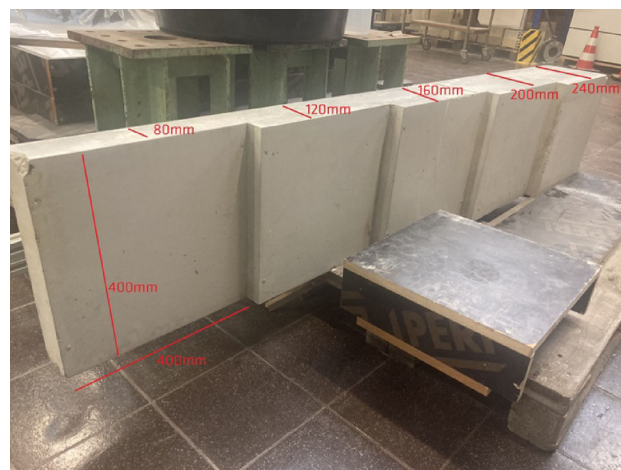


Fig. 4 Photo of the step wedge specimen lying on one side. In red, the dimensions are shown in millimeters (Photo: BAM)

increments, i.e., the fifth and last step is 24 cm high (see Fig. 4). Only the first three steps were used in the experiment to determine whether the thickness frequency can be excited by hammer and laser impulse, whereas only the first step can be considered a plate with a lateral extension to thickness ratio of 5:1. We used PCB 352C33 and PCB 352M66 accelerometers, a PCB 378B03 microphone, and the LDV as sensors to record the hammer excitation. For the laser excitation, we had to discard the microphone because we could not mount it on the vertical surface alongside the laser beam and used only the accelerometers and LDV. Sensors were placed in the plate center, and hammer and laser excitation occurred at a 3 cm separation using the surface configuration.

3 Results

3.1 Energy and Frequency Content

Signal energy is measured on the backside of the cube sample using an accelerometer, and the integral area up to 250 kHz of the associated FFT amplitude spectrum is computed. For the case of the 5 mm steel ball source, the integrated amplitude value is 10.0, and when this is divided by the (1.3 ± 0.2) mJ impact energy, we obtain an integral area of 7.7 (+ 1.4/– 1.0) per mJ. The results from all wave sources are computed in this manner and presented in Table 2. The mean integral area for all three mechanical impactors is 4.4 (+ 0.7/– 0.5) per mJ. To obtain the energy that the laser transfers into the specimen, we divide the laser integral area of 0.29 by the integral area of 4.4 (+ 0.7/– 0.5) per mJ from the mechanical impactors, which gives a laser energy of $(0.07 + 0/– 0.1)$ mJ. The experimentally determined transferred laser energy of $0.07 + 0/– 0.1$ mJ divided by the nominal laser energy of

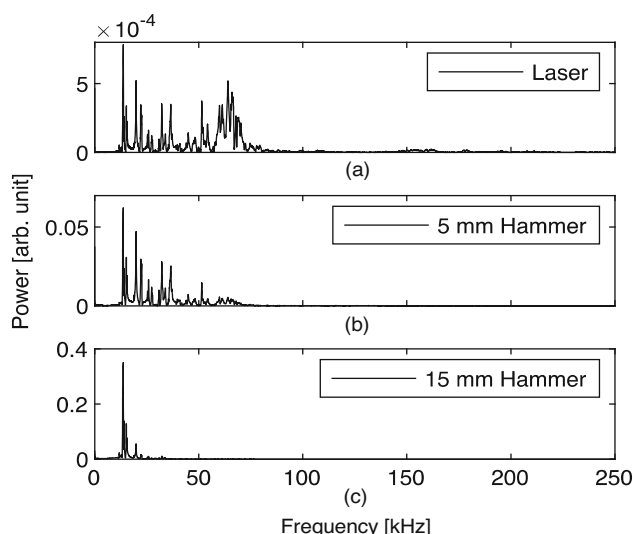


Fig. 5 Backside test configuration: frequencies excited by **a** laser ablation, **b** 5 mm, and **c** 15 mm steel ball hammer. Signals were measured with a PCB 352C33 accelerometer on the backside of the 15 cm concrete cube. The laser ablation excites frequencies in the range of (0 to 80) kHz, while 5 mm and 15 mm steel ball hammers excite frequencies in the range of (0 to 70) kHz and (0 to 25) kHz, respectively. All spectra have their highest peak at 13.7 kHz, one of the cubes' natural frequencies. Note the different y-axis scales

150 mJ results to obtain a relative energy transfer of 0.4 to 0.5%.

Frequencies generated by laser ablation in the range of (0 to 80) kHz can be measured on the backside of the cube the PCB 352C33 accelerometer (Fig. 5). The 5 mm hammer excites frequencies in the range of (0 to 70) kHz, whereas the frequencies generated by the 15 mm hammer lie in the range of (0 to 25) kHz. The maximum power of the FFT is 8×10^{-4} V for the laser, 0.06 for the 5 mm hammer, and 0.35 for the 15 mm hammer. Further, we can see that the laser and the hammers excite one of the cubes' natural frequencies at 13.7 kHz, which we verified by a natural frequency simulation. This natural frequency strongly dominates the spectra, which is why frequencies below 13.7 kHz are not clearly visible.

Figure 6 shows the time signals using the laser ablation, 5 mm, and 15 mm steel ball hammer excitation sources where

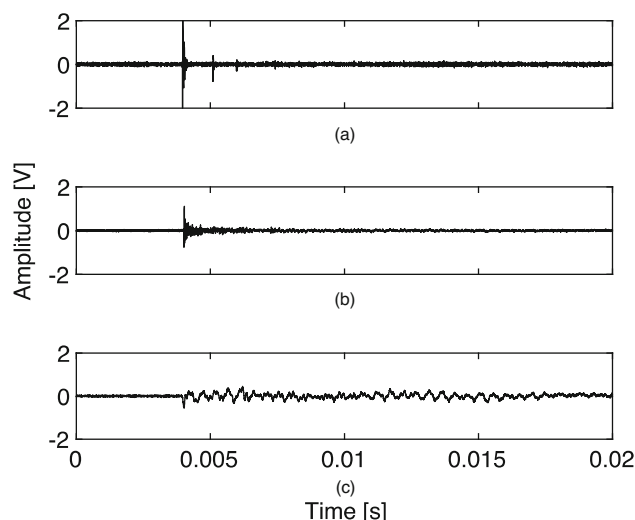


Fig. 6 Time signals of **a** laser ablation, **b** 5 mm, and **c** 15 mm steel ball hammer on the surface of the 15 cm thick concrete plate measured at 3 cm separation from the point of impact using an LDV

the signals are recorded using the LDV. The laser signal duration is the shortest, with less than 1 ms and shows a sharp peak. The 5 mm hammer vibration lasts 4 ms and shows a clear signal onset and decay similar to the laser. The 15 mm hammer vibration lasts over the entire signal length, but its onset is less sharp, and no clear decay is visible.

When measuring the signal on the surface of the intact plate with the LDV, the integral area of the laser is 1.45 and lies between that of the 8 mm and 10 mm hammer. We do not relate this integral area to the potential energy because a hammer was used instead of a steel ball drop, and it is not possible to assume that the ball drop and hammer strike have the same power. Comparing the hammer and laser integral area on the surface of the intact plate next to the receiver with that on the backside of the cube, we see that less laser energy reaches the backside. By contrast, the laser energy on the surface is comparable to the 8 mm and 10 mm hammer. From Fig. 7, we conclude that the laser ablation generates a broad frequency band in the range of (0 to 150) kHz when measured on the surface close to the sensor. In contrast, the 5 mm and 15 mm hammers excite frequencies between (0 to 50) kHz and (0 to 20) kHz, respectively.

Table 2 Potential energy and maximum usable frequency of steel balls and laser

Excitation	E_{pot} (mJ) cube	f_{max} (kHz)	Int area cube	Integral area/mJ
5 mm steel ball	1.3 ± 0.2	29.1	10.0	7.7 (+ 1.4/- 1.0)
8 mm steel ball	6 ± 0.5	36.4	18.1	3.0 (+ 0.3/- 0.2)
10 mm steel ball	11.2 ± 1.2	58.2	28.6	2.6 (\pm 0.3)
1064 nm Nd:YAG laser, $E_l = 150$ mJ, $\tau_l = 7$ ns	0.07 (+ 0/- 0.1)	80 to 150	0.29	4.1 (+ 0.7/- 0)

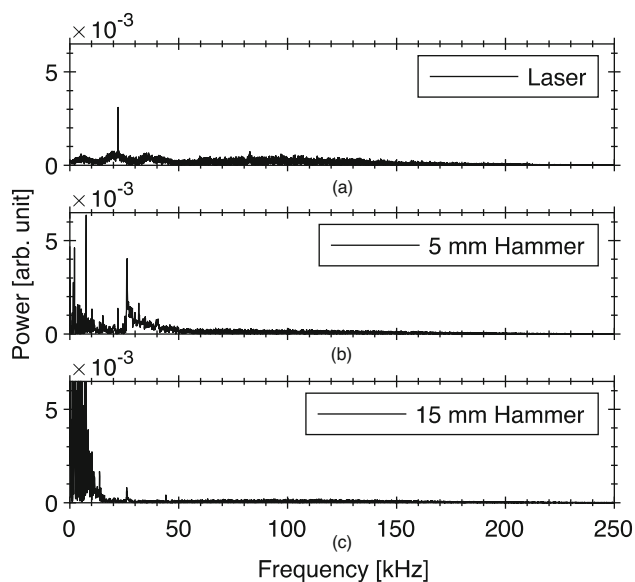


Fig. 7 Surface test configuration: frequencies excited by **a** laser ablation, **b** 5 mm, and **c** 15 mm steel ball hammer impulse measured by LDV on the surface of the 15 cm thick intact plate at 3 cm separation from the point of excitation. The laser ablation shows evenly distributed power in the range of (0 to 150) kHz. The 5 mm steel ball hammer excites frequencies in the range of (0 to 50) kHz, while the 15 mm steel ball hammer excites frequencies in the range of (0 to 20) kHz

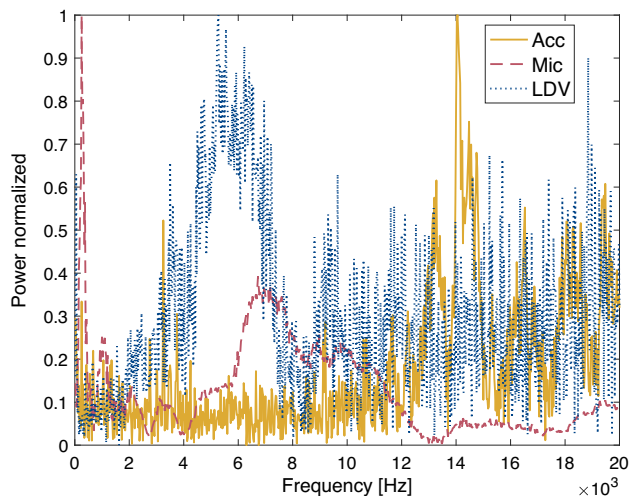


Fig. 8 Mean FFT of 49 signals recorded by PCB 352C33 accelerometer (Acc), PCB 378B02 microphone (Mic), and laser Doppler vibrometer (LDV). Excitation by laser impulse is located at the plate center of the 15 cm thick intact plate specimen using the surface configuration. Signal recorded at 10 cm separation. The accelerometer shows its highest peak at 14.7 kHz, the microphone at 250 Hz, and the LDV at 5250 Hz

3.2 Intact Plate

The mean frequency spectra of 49 signals excited by laser impulse are shown in Fig. 8. The accelerometer records its highest peak at 14.7 kHz, close to the expected thickness

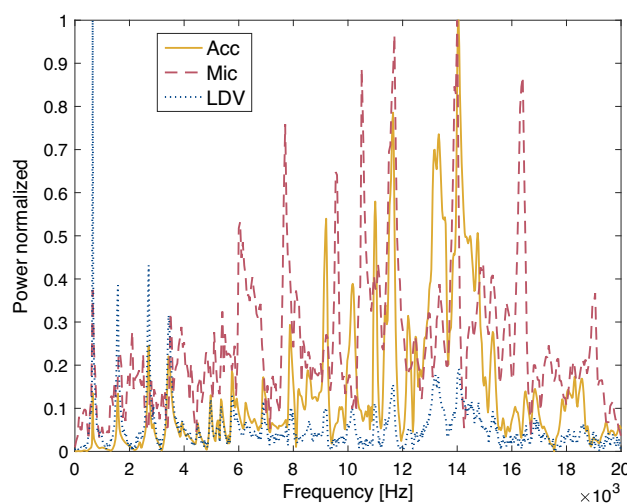


Fig. 9 Mean FFT of 46 signals recorded by PCB 352C33 accelerometer (Acc), PCB 378B02 microphone (Mic), and laser Doppler vibrometer (LDV). Impulse from the 15 mm steel ball hammer is located at the plate center of the 15 cm thick intact plate using the surface configuration. Signal recorded at 10 cm separation. The expected thickness resonance frequency is visible at approximately 14 kHz as the highest peak for both the accelerometer and microphone. The LDV also shows a peak at 14 kHz, but its highest peak is at 650 Hz

resonance frequency. The microphone and the LDV show their highest peaks at 250 Hz and 5250 Hz, respectively. The accelerometer is thus the only sensor that records the thickness resonance frequency when excited by laser impulse. We relate the 250 Hz component of the microphone to the loud ablation bang. The LDV might have suffered from reflectivity issues which could be why it did not record the thickness resonance frequency. In comparison to the laser excitation, Fig. 9 shows the mean frequency spectra of 46 signals excited by a 15 mm hammer impulse. The accelerometer and microphone have their maximum peaks at 14 kHz. The LDV shows a peak at 14 kHz as well, but its highest peak is at 650 Hz. The 650 Hz component is also visible in the other two sensors but with less power alongside other modal vibrations that are recorded by all sensors. All single measurements combined into a 2-D scan can be seen in Fig. 10. The signals are measured with the accelerometer, and the FFTs for each location are normalized and color-coded: yellow stands for the highest power and blue for the lowest. In the plate center at position 50 cm, the thickness resonance frequency is visible at 14 kHz when excited by the 15 mm hammer (see Fig. 10a). At the plate sides, the maximum frequency drops to 12.5 kHz. Figure 10b shows the results of the laser excitation. No continuous frequency band at the expected 14 kHz thickness resonance frequency is visible. Only at position 60 cm, one measurement shows its peak at 14.7 kHz.

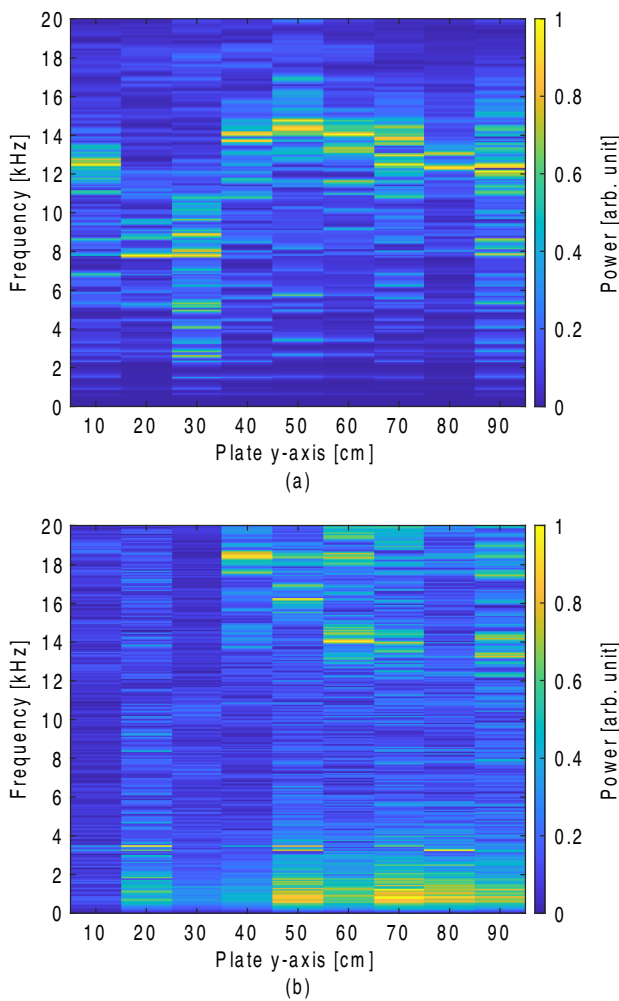


Fig. 10 2-D IE-scan of the 15 cm thick intact plate in the y-direction. Excitation from 15 mm steel ball hammer (a) and laser (b) recorded by a PCB 352C33 accelerometer at 10 cm separation. The hammer excites the expected thickness resonance stretch frequency at approximately 14 kHz in the plate center at $y = 50$ cm. The laser excitation excites a 14.7 kHz frequency at $y = 60$ cm but nowhere else. Other frequency peaks are below 2 kHz or above 16 kHz

3.3 Delaminated Plate

The signals generated by hammer and laser excitation, recorded with the accelerometer, can be found in Figs. 11 and 12, respectively. The hammer-generated signal shows a vibration that lasts over the entire signal length. In comparison, the laser excitation signal shows a vibration only for 2 ms after signal onset. The average maximum amplitude of the 38 hammer signals is 3.03 V. On the contrary, the average maximum amplitude of the 14 laser signals is 0.11 V, which is 28 times lower than that of the hammer. The results of the 1-D continuous wavelet transformation (CWT) are shown in Figs. 11 and 12 for hammer and laser excitation, respectively. The frequency and energy distribution over time show that

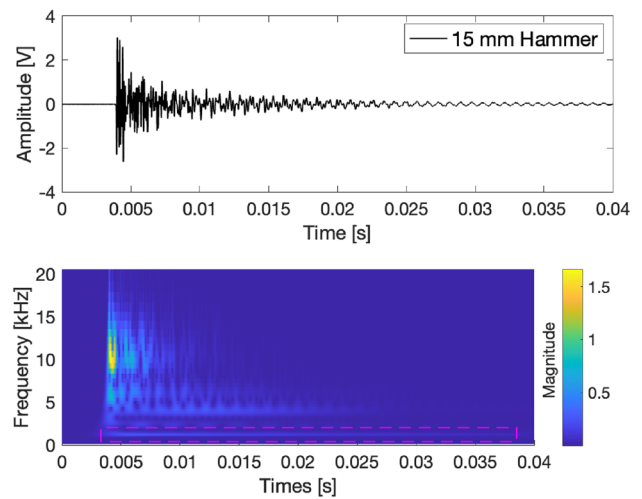


Fig. 11 1-D-CWT of the hammer signal recorded by PCB 352C33 accelerometer at the center of the 15 cm thick delaminated plate. The signal shows vibrations over the whole length of the signal. The CWT shows the highest energy at frequencies around 10 kHz at signal onset. The 1250 Hz flexural frequency band is visible at the bottom (marked in pink, dashed rectangle)

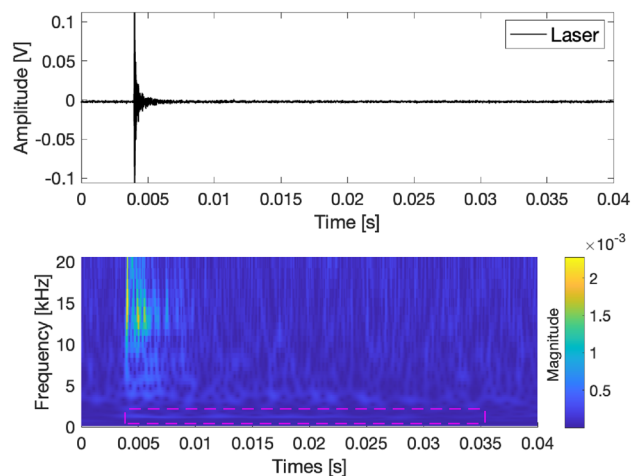


Fig. 12 1-D-CWT of the laser signal recorded by PCB 352C33 accelerometer at the center of the 15 cm thick delaminated plate. The laser signal shows vibrations only for 2 ms after the signal onset. The CWT shows the highest energy at frequencies around 15 kHz at signal onset. The 1250 Hz flexural frequency band is only faintly visible at the bottom (marked in pink, dashed rectangle)

most of the hammers' excitation energy is present in frequencies around 10 kHz. The 1250 Hz flexural vibration can be seen at the bottom of the plot, framed in a pink, dashed rectangle. In the first 6 ms after signal onset, the high energy vibrations at about 10 kHz dominate over the low frequencies. After the high frequencies vanish, the low-frequency flexural vibrations stand out. The signal duration and the duration of the 1250 Hz frequency band are similar. The CWT of the

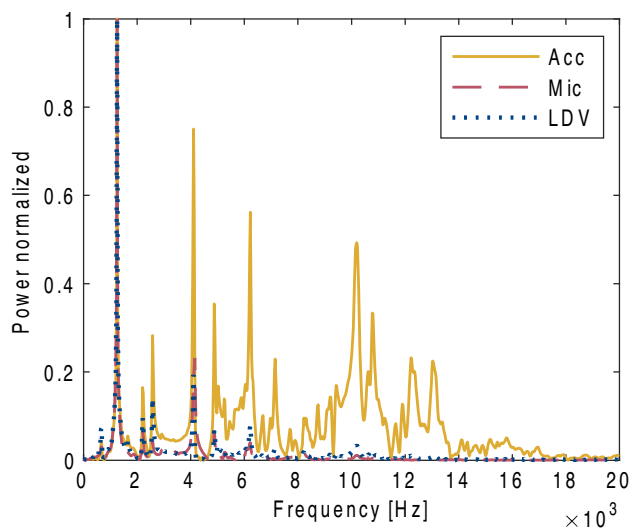


Fig. 13 Mean FFT of 38 signals recorded by PCB 352C33 accelerometer (Acc), PCB 378B02 microphone (Mic), and Laser-Doppler Vibrometer (LDV). Impulse from the 15 mm steel tip hammer is located at the plate center of the 15 cm thick delaminated plate using the surface test configuration. Signal recorded at 10 cm separation. No thickness resonance frequency, expected at approximately 14 kHz, is visible. Instead, low-frequency flexural vibrations can be seen at 1250 Hz and 4100 Hz for all three sensors

laser signals shows that most energy is present in frequencies around 15 kHz. The low-frequency flexural vibration at 1250 Hz is only faintly visible. From Fig. 12, we see that the signal duration of the laser signal is about 2 ms while the 1250 Hz frequency band of the CWT lasts for 20 ms, ten times as long.

Figure 13 shows the mean frequency spectra of 38 hammer impulse signals collected using the surface configuration. A flexural vibration at 1250 Hz can be seen for all three sensors. Further, a higher-order vibration mode can be seen at 4100 Hz in all sensors. All sensors are thus capable of measuring low-frequency flexural vibration modes when excited by the hammer. For comparison, Fig. 14 shows the mean frequency spectra of 14 laser impulse signals collected using the surface configuration. The flexural vibration at 1250 Hz can only be seen for the accelerometer and LDV but not for the microphone. The microphone has its highest peak at 275 Hz. The 2-D scan across the delaminated plate with hammer and laser excitation is displayed in Fig. 15. Above the delamination, between 30 and 70 cm, the thickness resonance frequency disappears, and instead, a low-frequency flexural vibration can be seen at 4100 Hz. Between 50 and 60 cm, the lowest vibration mode of 1250 Hz is visible for both hammer and laser excitation. While the hammer excitation shows the thickness resonance frequency aside from the delamination, the laser excitation only shows the flexural vibrations. Since the energy of the low-frequency flexural vibrations from the

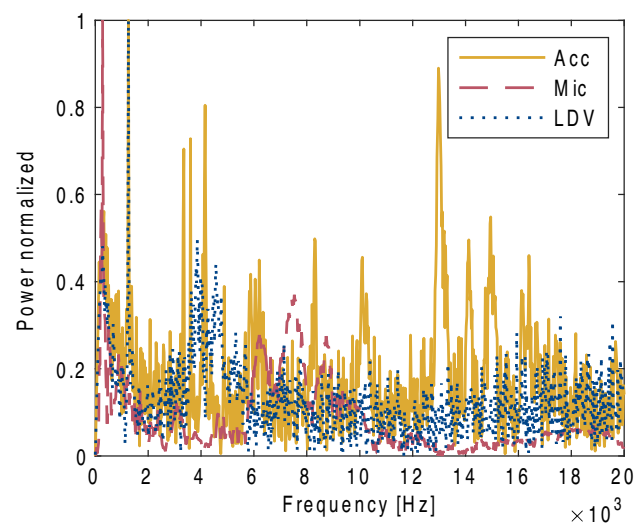
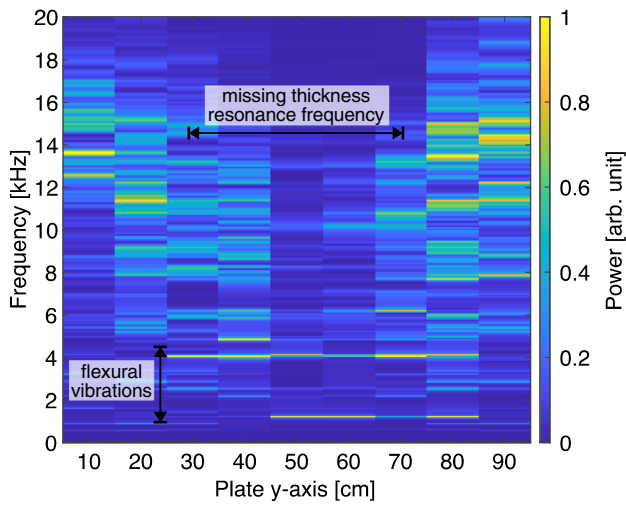


Fig. 14 Mean FFT of 14 signals recorded by PCB 352C33 accelerometer (Acc), PCB 378B02 microphone (Mic), and laser Doppler vibrometer (LDV) using the surface test configuration. Excitation from laser impulse is located at the plate center of the 15 cm thick delaminated plate. Signal recorded at 10 cm separation. No thickness resonance frequency expected at approximately 14 kHz is visible. Instead, a low-frequency flexural vibration can be seen at 1250 Hz for the accelerometer and LDV but not for the microphone

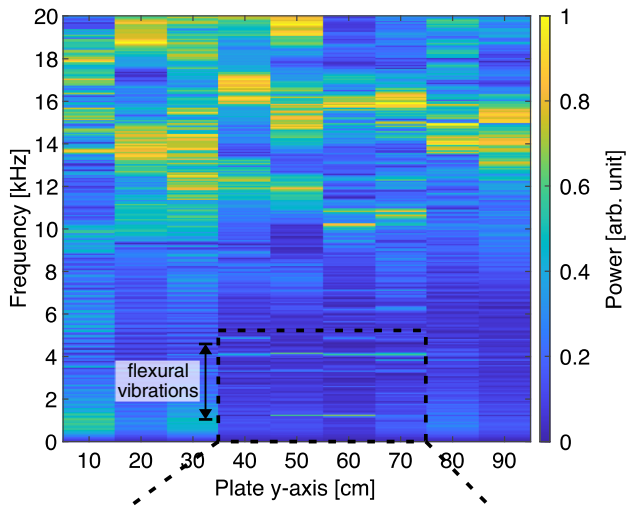
laser excitation is so small, Fig. 15c shows a magnified portion of the plate. None of the sensors could measure the expected thickness resonance frequency of the 3 cm thick delaminated part of approximately 70 kHz. The numerical vibration analysis of the delaminated slab ($40 \times 40 \times 3$) cm correlates well with the measured results (see Fig. 16). The first natural frequency is found at 1285 Hz, a 35 Hz difference from the measured experimental value of 1250 Hz. The following natural frequencies are 2524 Hz, 3608 Hz, 4308 Hz, 4340 Hz, and 5271 Hz. Analyzing the deformation location of the first six natural frequencies shows that the first and the fifth have their highest displacement at the plate center where the accelerometer was placed. Therefore, we conclude that the fifth natural frequency at 4340 Hz corresponds to the measured 4100 Hz.

3.4 Steel-Reinforced Slab

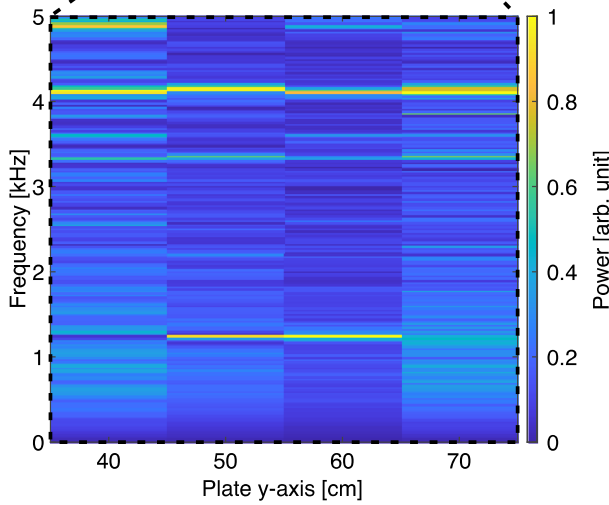
Figure 17a shows a 2-D scan along the y-direction in the slab center with hammer excitation by the Olson CTG-2 concrete thickness gauge. Between (5 to 15) cm and (40 to 70) cm, the thickness resonance frequency at approximately 10 kHz is visible. At the location of the metal tendon duct at $y = 30$ cm, frequencies at 7.8 kHz are visible at $y = (25$ to 40) cm. At the location of the Styrofoam plate, that is, along the y-axis position from (75 to 105) cm, the thickness resonance frequency band is missing. Instead, the thickness resonance frequency of the 15 cm thick delaminated area can be seen at 13.8 kHz.



(a)



(b)



(c)

Fig. 15 2-D IE-scan of the 15 cm thick delaminated plate in the y-direction. Excitation from 15 mm hammer (a) and laser (b, c), where c is a magnified sub-section of b. Signals were recorded by a PCB 352C33 accelerometer at 10 cm separation. At position $y = (30 \text{ to } 70)$ cm of the artificial delamination, the 14 kHz thickness resonance frequency is missing, and instead, low flexural vibrations at 1250 Hz and 4100 Hz are present; this is visible with both hammer and laser excitation. The frequency peaks of the flexural vibrations are very narrow (see Fig. 14), as seen in c

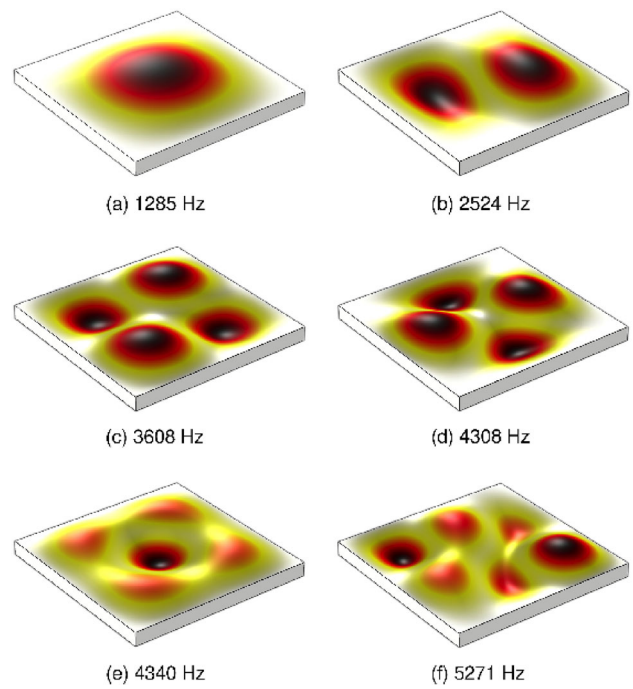


Fig. 16 Mode shapes of the first six natural frequencies of the delamination in the delaminated plate. The natural frequencies (a) 1285 Hz and (e) 4340 Hz could be verified experimentally. The plate dimension is $(40 \times 40 \times 3)$ cm

Figure 17b shows a 2-D scan along the y-direction in the plate center with laser excitation. Compared to the hammer excitation, no thickness resonance frequency is visible at 10 kHz for laser excitation. Most of the power seems to be randomly distributed in the frequency range from (16 to 20) kHz. This demonstrates that the 15 cm deep delamination in the specimen can be detected using the hammer but not with the laser excitation. Further, at the location of the empty tendon duct, no low frequencies can be seen.

3.5 Step Wedge

In the following, only the results for the PCB 352C33 accelerometer excited with a 5 mm steel ball hammer and laser are shown. The 8 cm thick first step (Fig. 18) has a calculated thickness resonance frequency of 26.6 kHz, which is measured when struck with a 5 mm hammer at 26.1 kHz. A second high and sharp peak at 7475 Hz is present in the spectrum. The laser ablation does not excite the thickness resonance frequency but shows its highest frequency peak at 20.2 kHz. With a thickness to lateral extension ratio of 1/5, the first step of the step wedge specimen can be seen as a plate. The thicker steps are not seen as plates, so their results are not displayed. However, we can state that the thickness resonance frequency could not be excited using the laser source at steps two and three. In comparison, the hammer could excite

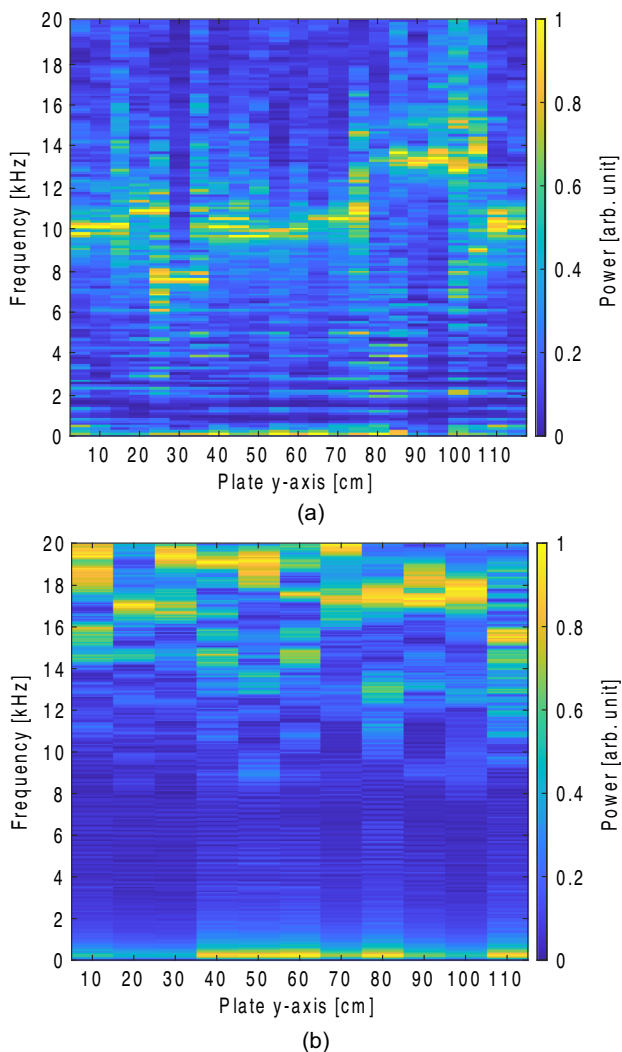


Fig. 17 2-D IE scan of the 20 cm thick steel-reinforced slab in the y-direction. Excitation by hammer (a) and laser (b). Signal recorded by a PCB 352C33 accelerometer at 10 cm separation. The hammer excites the expected thickness resonance frequency of the plate of 10 kHz at positions $y = (5 \text{ to } 15 \text{ and } 40 \text{ to } 75) \text{ cm}$. At the position of the tendon duct at $y = 30 \text{ cm}$, frequencies at 7.8 kHz are visible. At the position of the artificial delamination at $y = (75 \text{ to } 105) \text{ cm}$ in 15 cm depth, the thickness resonance frequency is missing. Instead, the thickness resonance frequency of the 15 cm thick delamination at 13.8 kHz is visible. The laser does not excite the thickness resonance frequency, and most of the frequency peaks are above 16 kHz. No flexural vibration modes can be seen here. Data for a obtained from Aßmann and Bühling [30]

the thickness resonance frequency at these steps. The experiment shows that the thickness resonance frequency cannot be excited by a laser impulse even for the thinnest 8 cm first step of the specimen. By contrast, the hammer accurately excites the thickness resonance frequency with distinct, easy-to-identify peaks in the FFT.

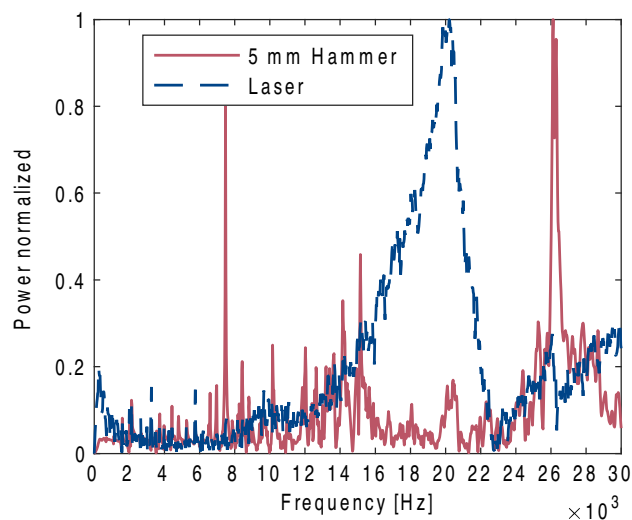


Fig. 18 Mean FFT of 59 laser signals and 24 hammer signals measured at the 8 cm thick first step of the step wedge specimen. The 5 mm hammer excites the thickness resonance frequency at 26.1 kHz. The laser does not excite the thickness resonance frequency but shows its highest peak at 20.2 kHz

4 Discussion

The experimental results show that a laser source can excite low-frequency flexural vibrations in concrete over a shallow delamination. However, the full-thickness stretch resonance frequency could only reliably be detected when using mechanical hammer excitation. In the center of the intact plate, the laser was able to excite the thickness stretch resonance frequency. However, this excitation was only visible at one test location at the plate, and not in other specimens, which is why we abstain from stating that the laser ablation can excite the thickness resonance. The laser ablation energy transfer into the specimen is a factor of 15 (5 mm steel ball) to 177 (10 mm steel ball) less compared to the mechanical impact. We suggest that this is the main reason why the thickness resonance frequency is essentially not excited by the laser excitation. Furthermore, the effect of the wave energy radiation pattern of the laser source needs to be further investigated in future studies to see if the laser ablation exhibits more, less, or equal energy on the surface than into the body. The frequencies excited by the laser have a broader frequency spectrum but lower energy content compared to the hammer impacts (Figs. 5 and 7). Because wave attenuation is a leading cause of energy loss and acts on each cycle of vibration, a rapid loss of energy results from the already low initial energy input [7]. The signal can be recorded most reliably and with the greatest sensitivity using a surface-mounted accelerometer. Non-contact sensors such as microphones and the laser Doppler vibrometer do not always record the expected resonance frequency and are subject to higher noise levels. The

LDV experienced issues with poor surface reflectivity and surface roughness of concrete. Nevertheless, for non-contact detection, the laser Doppler vibrometer is the better choice for two reasons: (1) it can be used at significant offset distances, for example, in tunnel settings, and it is not influenced by the noise from ablation at the surface, and (2) contactless acoustic sensors may be disrupted by acoustic noise owing to the ablation process, while LDVs are not because they directly measure the surface movement. Although laser ablation damages the concrete surface at the microscopic scale, we still consider the method as essentially non-destructive. The damage is minimal, and no cracks have been observed to emerge from the ablation location. This observation is supported by others: experiments using laser ablation inductively coupled plasma mass spectrometry (LA-ICP-MS), where laser ablation is used for the material characterization of concrete samples, did not show cracks caused by ablation [31]. During the casting process of the concrete specimens, we had difficulties positioning the Styrofoam plate at precisely 3 cm depth because the plate was not externally fixed. Therefore, the defect plate might have moved while pouring the concrete. During the laser experiments, we experienced difficulties related to the rough surface of the concrete. Changes in focal length of a few millimeters caused by surface roughness led to an unfocused laser spot. An unfocused laser spot can be detected immediately during the experiment as the volume of the ablation decreases and is indicated by a lower amplitude signal. The correct focal length can be ensured by a precise distance measurement and a lens height adjustment. Using a longer focal length would lead to a longer focal point, making defocusing less of a problem. The interaction of the laser beam with concrete is a complex process, as the surface consists of many different mineralogical phases and geometric shapes. In our experiments, the concrete surface color for all four specimens was light gray, owing to a covering layer of cement paste at the surface. We expect to find exposed coarse aggregates on the surface of real-life concrete road surfaces because of wearing degradation by passing vehicles. The different material properties of the aggregates result in changes in the laser ablation threshold; consequently, energies and frequencies transferred to the specimen could be affected. During the laser ablation experiments, we occasionally experienced a sudden decrease in signal amplitude. This was caused by fine dust owing to the ablation event that covered the focusing lens and hindered the passage of light through the lens. Laser ablation dust and other airborne contamination of sensitive optical instruments must be avoided. In the worst case, this can lead to the destruction of the lens and unwanted lateral laser light reflections that could be harmful to humans.

5 Conclusions

This study investigated the use of a laser ablation impact echo technique to find delaminations in concrete plates. As part of this work, the frequency and energy transfer from the laser excitation into concrete specimens were studied. We have shown that a laser impulse that causes surface ablation in concrete can be used to excite low-frequency vibrations over a shallow, 3 cm deep artificial delamination in a concrete plate, i.e., we were able to detect the delamination using laser ablation using the impact echo technique. These low-frequency flexural vibrations can be measured with both surface-mounted accelerometers and contactless laser Doppler vibrometers. The accelerometer provides a higher signal-to-noise ratio but requires surface contact. The LDV is contactless, but its sensitivity is negatively affected by the rough concrete surface and its poor surface reflectivity. However, the full thickness resonance frequency generated by laser impulse could not be measured, not even in a plate as thin as 8 cm. Similarly, deeper delaminations, such as the 15 cm Styrofoam plate in the steel-reinforced slab, could not be detected by laser-induced impact echo. The findings were compared and verified by using steel hammers as mechanical-type impulse actuators. Using mechanical impulse excitation, we were able to detect all delaminations and also excite the thickness resonance frequency in all specimens. The frequencies excited by laser ablation in the specimens range from 0 to 150 kHz as measured on the surface at 3 cm separation from the excitation point. After traveling through 15 cm in concrete, however, the frequency range excited by laser ablation reduces to 0 kHz to 80 kHz. Consequently, the laser ablations' inability to generate the thickness resonance frequency vibration arises from the low energy input. The necessary frequencies are present, however, with insufficient energy. A more powerful laser ablation source should be studied to confirm this hypothesis. Further studies should also focus on a general formulation of laser-concrete interaction for elastic wave generation to better understand the input energy limits and wave energy partition of laser-based excitation for concrete. Furthermore, the influence of varying laser wavelengths and pulse durations should be investigated.

Acknowledgements The work reported in this manuscript is supported by the TUM International Graduate School of Science and Engineering (IGSSE). The authors are thankful for the valuable contributions of Sebastian Münchmeyer, an electrical engineer at the institute, who built the laser platform and installed the laser safety measures. Further, we are grateful for the valuable contributions of the project partners at BERNARD Ingenieure GmbH, namely, Dr. Sonja Dallinger and Jost Mazur as well as Dr. Dirk Püschel from Soundtec GmbH. The authors would like to thank the German Federal Ministry for Economic Affairs and Energy for funding the project under grant number 4561201.

Author Contributions Conceptualization: CUG, JFS, JK; methodology: CUG, JFS, JK; formal analysis and investigation: JFS, BB, JK; writing—original draft preparation: JFS, writing—review and editing: JSP, JK, BB, CUG; funding acquisition: CUG; resources: CUG, BB; supervision: CUG, JSP; visualization: JFS; software: JFS.

Funding Open Access funding enabled and organized by Projekt DEAL. This work was funded by the funding program "Central Innovation Program for small and medium-sized enterprises (SMEs)" of the Federal Ministry for Economic Affairs and Energy in Germany under Grant Agreement No 4561201 and the International Graduate School of Science and Engineering (IGSSE) of the Technical University of Munich (Project Team 14.02).

Availability of Data and Material The datasets generated during and analyzed during the current study are available from the corresponding author on reasonable request.

Code Availability The code that supports the findings of this study is available from the corresponding author upon reasonable request.

Declarations

Conflicts of interest The authors have no competing interests to declare that are relevant to the content of this article. The authors declare they have no financial or non-financial interests to disclose.

Open Access This article is licensed under a Creative Commons Attribution 4.0 International License, which permits use, sharing, adaptation, distribution and reproduction in any medium or format, as long as you give appropriate credit to the original author(s) and the source, provide a link to the Creative Commons licence, and indicate if changes were made. The images or other third party material in this article are included in the article's Creative Commons licence, unless indicated otherwise in a credit line to the material. If material is not included in the article's Creative Commons licence and your intended use is not permitted by statutory regulation or exceeds the permitted use, you will need to obtain permission directly from the copyright holder. To view a copy of this licence, visit <http://creativecommons.org/licenses/by/4.0/>.

References

- Sansalone, M., Carino, N.J.: Detecting delaminations in concrete slabs with and without overlays using the impact-echo method. *Mater. J.* **86**, 175–184 (1989)
- Guthrie, W.S., Larsen, J.L., Baxter, J.S., et al.: Automated air-coupled impact-echo testing of a concrete bridge deck from a continuously moving platform. *J. Nondestr. Eval.* **38**, 1–8 (2019)
- Groschup, R., Grosse, C.U.: MEMS microphone array sensor for air-coupled impact-echo. *Sensors* **15**, 14932–14945 (2015)
- Scherr, J.F., Grosse, C.U.: Delamination detection on a concrete bridge deck using impact echo scanning. *Struct. Concr.* **22**, 806–812 (2021)
- Prada, C., Balogun, O., Murray, T.W.: Laser-based ultrasonic generation and detection of zero-group velocity Lamb waves in thin plates. *Appl. Phys. Lett.* **87**, 194109 (2005)
- Jacobs, L.J., Whitcomb, R.W.: Laser generation and detection of ultrasound in concrete. *J. Nondestr. Eval.* **16**, 57–65 (1997)
- Jacobs, L.J., Owino, J.O.: Effect of aggregate size on attenuation of rayleigh surface waves in cement-based materials. *J. Eng. Mech.* **126**, 1124–1130 (2000)
- Mori, K., Spagnoli, A., Murakami, Y., et al.: A new non-contacting non-destructive testing method for defect detection in concrete. *NDT and E Int.* **35**, 399–406 (2002)
- Dai, X., Zhu, J., Haberman, M.R.: A focused electric spark source for non-contact stress wave excitation in solids. *J. Acoust. Soc. Am.* **134**, EL513–EL519 (2013)
- Dai, X., Zhu, J., Tsai, Y.-T., et al.: Use of parabolic reflector to amplify in-air signals generated during impact-echo testing. *J. Acoust. Soc. Am.* **130**, EL167–EL172 (2011)
- Kaczmarek, M., Piwakowski, B., Drellich, R.: Noncontact ultrasonic non-destructive techniques: state of the art and their use in civil engineering. *J. Infrastruct. Syst.* **23**, B4016003 (2017)
- Gibson, A., Popovics, J.S.: Lamb wave basis for impact-echo method analysis. *J. Eng. Mech.* **131**, 438–443 (2005)
- Oh, T., Popovics, J.S., Sim, S.-H.: Analysis of vibration for regions above rectangular delamination defects in solids. *J. Sound Vib.* **332**, 1766–1776 (2013)
- Oh, T., Popovics, J.S.: Practical visualization of local vibration data collected over large concrete elements. *Comput.-Aided Civ. Infrastruct. Eng.* **30**, 68–81 (2015)
- Sansalone, M.: Impact-echo: the complete story. *Struct. J.* **94**, 777–786 (1997)
- Sansalone, M., Carino, N.J.: Impact-echo: A Method for Flaw Detection in Concrete Using Transient Stress Waves. US Department of Commerce, National Bureau of Standards, Center for Building (1986)
- Algernon, D.: Impact-Echo: Analyse akustischer Wellen in Beton. In: Technische Universität Berlin, Fakultät VI - Planen Bauen Umwelt. Technische Universität Berlin, Berlin (2006)
- Bäuerle, D.: Laser Processing and Chemistry. Springer, Berlin (2013)
- Allmen, M.V., Blatter, A.: Laser-Beam Interactions with Materials: Physical Principles and Applications. Springer, New York (2013)
- Dewhurst, R., Edwards, C., Mckie, A., et al.: Estimation of the thickness of thin metal sheet using laser generated ultrasound. *Appl. Phys. Lett.* **51**, 1066–1068 (1987)
- Davies, S., Edwards, C., Taylor, G., et al.: Laser-generated ultrasound: its properties, mechanisms and multifarious applications. *J. Phys. D* **26**, 329 (1993)
- Pożar, T., Laloš, J., Babnik, A., et al.: Isolated detection of elastic waves driven by the momentum of light. *Nat. Commun.* **9**, 1–11 (2018)
- Rudolph, P.: Physikalische Chemie der Laser-Material-Wechselwirkung mit Ba-Al-Borosilikatglas, AlN, SiC, SiC-TiC-TiB₂. In: (2002)
- Poprawe, R.: Lasertechnik für die Fertigung. Springer (2005)
- Wilsch, G.: LIBS-Ein Tool zur Untersuchung der chemischen Zusammensetzung von Beton (2018)
- Mikami, K., Hasegawa, N., Kitamura, T., et al.: Characterization of laser-induced vibration on concrete surface toward highly efficient laser remote sensing. *Jpn. J. Appl. Phys.* **59**, 076502 (2020)
- Huber, A.: Dispersion Calculator (DC). In: German Aerospace Center (DLR) (2018). https://www.dlr.de/zlp/en/desktopdefault.aspx/tabid-14332/24874_read-61142/. Accessed 28 June 2021
- Zhu, J., Popovics, J.S.: Imaging concrete structures using air-coupled impact-echo. *J. Eng. Mech.* **133**, 628–640 (2007)
- Niederleithinger, E., Gardner, S., Kind, T., et al.: Muon tomography of the interior of a reinforced concrete block: first experimental proof of concept. *J. Nondestr. Eval.* **40**, 65 (2021)

30. Aßmann, N., Bühling, B.: Impact-Echo Dataset "Radarplatte". In:Harvard Dataverse (2021)
31. Decker, M., Siegel, J., Hilbig, H., et al.: LA-ICP-MS on hardened cement paste: laser-material interaction, signal formation and optimization of laser fluence. *Mater. Struct.* **54**, 144 (2021)

Publisher's Note Springer Nature remains neutral with regard to jurisdictional claims in published maps and institutional affiliations.